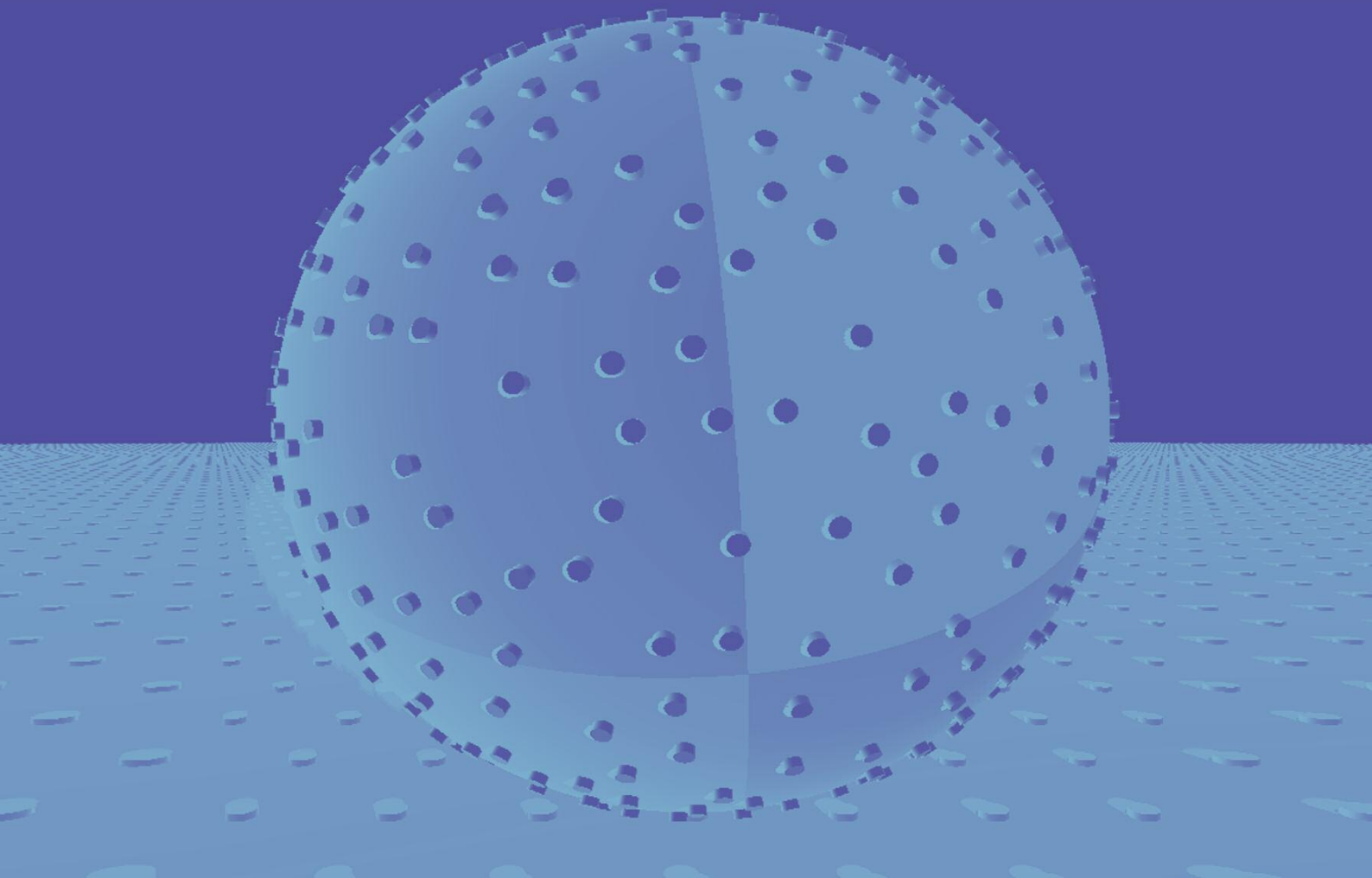




- Polymers and Proteins
- Carbohydrates
- Membranes and Vesicles
- Complex Systems

THEORY & BIO-SYSTEMS



Research in the Department of Theory & Bio-Systems

Das Leben besteht in der Bewegung.
Aristoteles



The main objective of our research activities is to understand the hidden dimensions of self-organization in biomimetic and biological systems. The molecular building blocks of these systems join "by themselves" and form a variety of supermolecular assemblies, which then interact to produce even larger structures and networks. Since these processes are difficult to observe experimentally on the relevant

length and time scales, theory and computer simulations are essential in order to integrate different experimental results into a coherent and unified framework. The department is also responsible for the International Max Planck Research School on "Biomimetic Systems".

The associates of the department form several research groups. At present, the research group leaders and topics are:

- *Rumiana Dimova*: Biophysics Lab;
- *Volker Knecht*: Molecular Dynamics;
- *Thomas Weigl*: Proteins and Membranes;
- *Mark Santer*: Carbohydrates and Polysaccharides;
- *Christian Seidel*: Polymers and Polyelectrolytes;
- *Angelo Valleriani*: Stochastic Processes;
- *Stefan Klumpp*: Regulation of Bioprocesses.

The main results of these research groups are described in separate reports on the following pages. These reports are related to four main topics: Polymers and proteins, carbohydrates, membranes and vesicles, as well as complex systems. Both carbohydrates and complex systems represent relatively new research fields in the department.

As far as membranes and vesicles are concerned, two particularly interesting results are about the cooperative binding of membrane-anchored receptors, see **Fig. 1** and separate report by *T. Weigl*, and the formation of membrane nanotubes induced by aqueous phase separation, see **Fig. 2** and my separate report.

Other topics that are only partially covered in the subsequent reports include the multiscale motility of molecular motors and the dynamics of filaments. In the following, I will briefly summarize our recent results on these topics.

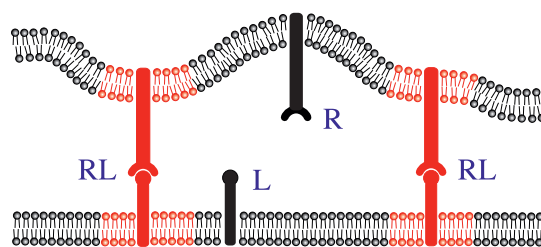


Figure 1: Cooperative binding of membrane-anchored receptors (R) and ligands (L). Binding requires that R and L are located opposite to each other and that the separation of the corresponding membrane segments matches the length of the RL-complexes.

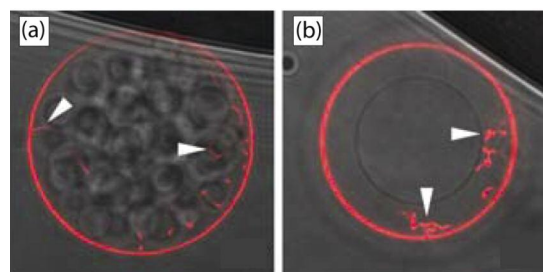


Figure 2: Membrane nanotubes within a lipid vesicle as indicated by the white arrows (a) during and (b) after aqueous phase separation within the vesicle. The fluorescently labeled membrane (red) forms both the large vesicle (outer circle), which has a diameter of about 40 μm , and the thin nanotubes, which have a thickness below optical resolution.

Motility of Molecular Motors.

We have focused on a particular class of molecular motors, namely motors that step along cytoskeletal filaments. Such stepping motors are essential for intracellular transport within eukaryotic cells as well as for their locomotion and division. All stepping motors have a similar molecular architecture with two identical motor domains, both of which are able to hydrolyze ATP into ADP and inorganic phosphate (Pi) as well as to dock onto the cytoskeletal filaments. In the last couple of years, we studied the multiscale motility of these motors on three different levels: conformational changes of motor proteins; free energy transduction by single motors; and cargo transport by motor teams.

Reinhard Lipowsky 11.11.1953

1978: Diploma, Physics,
(University of Heidelberg)

1982: PhD (Dr. rer. nat.), Physics
(University of Munich)

1979-1984: Teaching Associate
(University of Munich)

1984-1986: Research Associate
(Cornell University)

1986-1988: Group leader (FZ Jülich)

1987: Habilitation, Theoretical Physics
(University of Munich)

Thesis: Critical behavior of interfaces:
Wetting, surface melting and related
phenomena

1989-1990: Associate Professorship
(University of Munich)

1990-1993: Full Professorship
(University of Cologne), Director of the
Division "Theory II" (FZ Jülich)

Since Nov 1993: Director
(Max Planck Institute of Colloids and
Interfaces, Potsdam)

Conformational Changes of Motor Proteins.

When viewed with atomistic resolution, each motor domain of kinesin contains several subdomains: the nucleotide binding pocket, the microtubule binding site, and the neck linker, see **Fig. 3**. After ATP has been bound to the empty nucleotide binding pocket, it is hydrolyzed into ADP and Pi, both of which are successively released from the pocket. We have studied the associated conformational changes by atomistic Molecular Dynamics simulations, which revealed a certain allosteric coupling between the different subdomains (A. Krukau, V. Knecht).

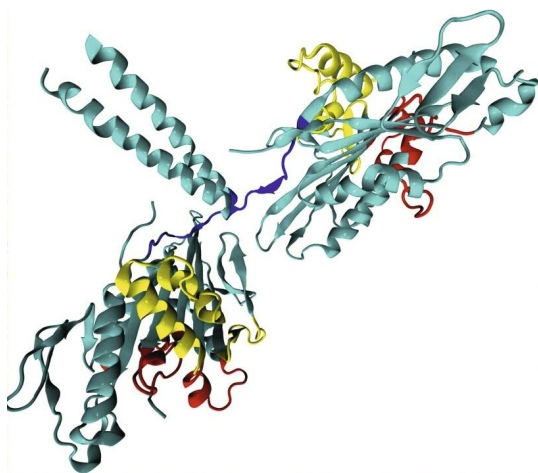


Figure 3: Two motor domains of kinesin (ribbon representation). Each motor domain contains a nucleotide binding pocket (red), a microtubule binding site (yellow), and a neck linker (blue). The „crosstalk“ between these different subdomains depends on the occupancy of the nucleotide binding pocket (empty, ATP, or ADP).

Free Energy Transduction by Single Motors.

Since each motor domain can exhibit three different nucleotide states, a dimeric motor with two such domains can attain nine such states. These states are connected by chemical and mechanical transitions and form a chemomechanical network with a large number of motor cycles. Such a representation has been used to integrate many experimental data for two different stepping motors, namely for kinesin in contact with microtubules (S. Liepelt, A. Valleriani) and for myosin V that walks along actin filaments (V. Bierbaum). Both kinesin and myosin V are characterized by a competition between several motor cycles.

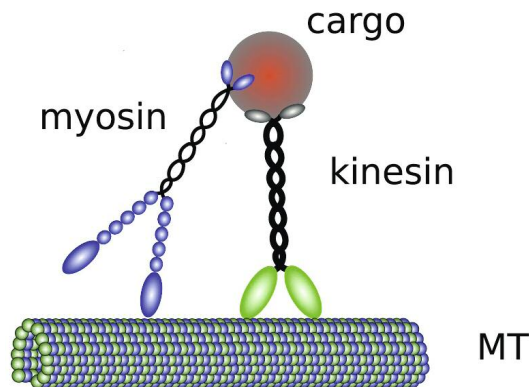


Figure 4: Cargo transport by the microtubule-based motor kinesin is enhanced by the actin-based motor myosin V. The latter motor binds to microtubules (MT) as well and then diffuses along these filaments. Vice versa, kinesin can bind to and diffuse along actin filaments. In this way, the two types of motors can transport the same cargo along both microtubules and actin filaments.

Cargo Transport by Motor Teams.

The transport of cargo within eukaryotic cells is performed by teams of molecular motors. Because each motor unbinds from the filament after a certain number of steps, the number of actively pulling motors varies with time. The case of two kinesins has been theoretically studied using two different representations of their state space (C. Keller, F. Berger, S. Klumpp, S. Liepelt). In some cases, cargo transport by one team of motors is enhanced by another team of motors that do not move in a directed manner but only diffuse along the filaments. One example is kinesin-driven cargo transport along microtubules that can be enhanced by the actin-based motor myosin V, see **Fig. 4** (F. Berger, M.J.I. Müller).

Depolymerization of Actin Filaments.

As mentioned, actin filaments provide the tracks for molecular motors such as myosin V. In addition, the polymerization and depolymerization of these filaments plays an essential role for many cellular processes such as cell division, locomotion, and adhesion. Quite recently, the depolymerization of single filaments was observed to be interrupted for extended periods of time. The interruptions are not coupled to ATP hydrolysis but arise from random modifications of actin promoters (T. Niedermayer).

For additional information about research at the Department of Theory & Bio-Systems, see subsequent reports and www.mpikg.mpg.de/th/

Reinhard Lipowsky
Director, Department of Theory & Bio-Systems

The Power of Polypeptides from a Molecular Perspective



Polypeptides (also called proteins) are linear biopolymers composed of amino acid residues that fold into well-defined structures depending on their amino acid sequence. Folding is essential for the function of a protein whereas misfolding can cause severe diseases. Our aim is to understand protein function and diseases on a molecular level. The information on the molecular dynamics

of polypeptides accessible experimentally is very limited. Therefore we employ molecular dynamics (MD) simulation techniques to model the process by which polypeptides sample conformational space. Here, the polypeptide and its solvent environment are described in atomic or near-atomic detail. Currently we try to understand how polypeptides may drag cellular organelles along filaments, recognize and kill bacteria as part of the immune defense, or cause neurodegenerative diseases.

Amyloid Peptides – Origin of Neurodegenerative Diseases

Amyloid diseases including Alzheimer's or Creutzfeldt-Jakob disease are associated with the conversion of a protein from a soluble (functional) form into higher order fibrillar aggregates rich in β -sheet structure. The toxic species, though, seemingly, are not the mature fibrils but early oligomers. To understand the origin of their toxicity and to develop drugs against amyloid diseases requires to comprehend the structure of these species. We study the folding and aggregation of small amyloid peptides in solution. The systems investigated include the model amyloid peptide B18 as in **Fig. 1**(a,b) **[1]**, as well as the 25-35 **[2]** and the 10-35 fragment of the Amyloid β (A β) peptide associated with Alzheimer's disease **[3]**, as in **Fig. 1**(c-e) and (f-k), respectively.

The amyloid peptides form various β -sheets consisting of different sets of residues with comparable statistical weight. Aggregation is largely driven by the hydrophobic effect. Disordered conformations are stabilized entropically whereas fibril-like, β -sheet rich structures exhibit a lower energy. The A β (10-35) dimers show a larger conformational diversity than observed in previous simulations using a (less accurate) implicit solvent model, highlighting the need of the (more accurate but also computationally more expensive) explicit solvent model. In a running project, we also study the full length A β (1-40) peptide in terms of the effect of an interface on the peptide's conformation and the peptide's ability to induce membrane pores, as a possible origin of its toxicity. In collaboration with Gerald Brezesinski, the structure of larger aggregates, peptide monolayers with β -sheet structure at a water/air interface, has been studied **[4]**.

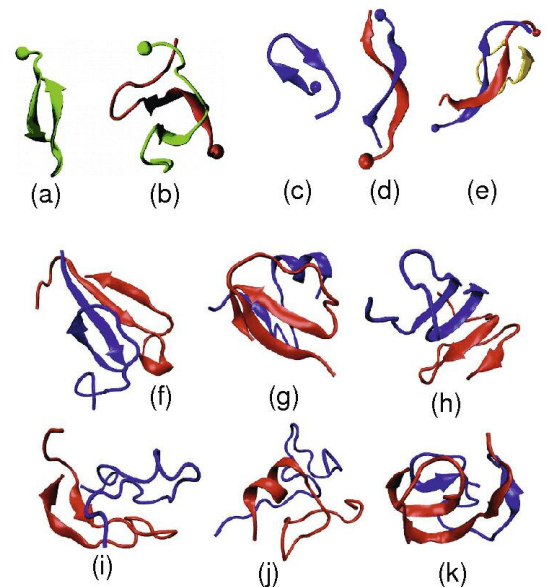


Fig. 1: β -hairpin folding and aggregation of fibrillogenic peptides in explicit water in molecular dynamics simulations. The model peptide B18 (a,b), as well as the A β (25-35) and A β (10-35) peptides associated with Alzheimer's disease, are depicted. In detail, (a) a B18 monomer **[1]** and (b) dimer **[1]**, (c) an A β (25-35) monomer, (d) dimer **[2]**, and (e) trimer, as well as (f-k) A β (10-35) dimers **[3]**, are shown in ribbon representation.

Antimicrobial Peptides – Smart Weapons of Immune Defense

Antimicrobial peptides (AMPs) are an evolutionary conserved component of the innate immune system found among all classes of life; their main function is the recognition and inactivation of invading pathogens like bacteria, viruses, or fungi. The mode of action of most AMPs is the permeabilization of the cell membrane via the formation of pores. AMPs are toxic against bacteria without affecting cells produced naturally in multicellular organisms, likely due to specific binding to lipids contained in the extracellular leaflet of pro- but not eukaryotic cell membranes. In vitro experiments of the antimicrobial peptide NK-2 indicate that the discrimination between zwitterionic lipids with phosphatidylethanolamine (PE) head groups exposed by prokaryotes and phosphatidylcholine (PC) head groups exposed by eukaryotes plays an important role. We have conducted molecular dynamics simulations in conjunction with a coarse grained model confirming that NK-2 binds more strongly to PE than to PC and revealing the underlying mechanism **[5]**. As indicated in **Fig. 2**, we find that the transfer of NK-2 from POPE to POPC is favored because of a better shielding of nonpolar groups from the water and increased electrostatic interactions

Volker Knecht 06.01.1970

1996: Diploma in Physics

(University of Kaiserslautern)

Thesis: Computer based renormalization group study of the two-dimensional XY model

1997: Software trainee

(TECMATH GmbH, Kaiserslautern)

1998-1999: Software engineer

(LMS Durability Technologies GmbH, Kaiserslautern)

2003: PhD, Physics (MPI of biophysical chemistry, Göttingen)

Thesis: Mechanical coupling via the membrane fusion SNARE protein syntaxin 1A: a molecular dynamics study

2003-2005: Postdoc

(University of Groningen, the Netherlands)

2005-2006: Postdoc

(MPI of Colloids and Interfaces, Potsdam)

Since 2006: Group Leader

(MPI of Colloids and Interfaces, Potsdam)

between the cationic and anionic portions of the lipid head-groups. We also find that the adsorption of a cationic peptide to an anionic lipid is governed by a complex interplay of competing interactions. In a related project we reveal the driving forces of molecular recognition of pathogens in the form of proteins or lipids by antibodies [6].

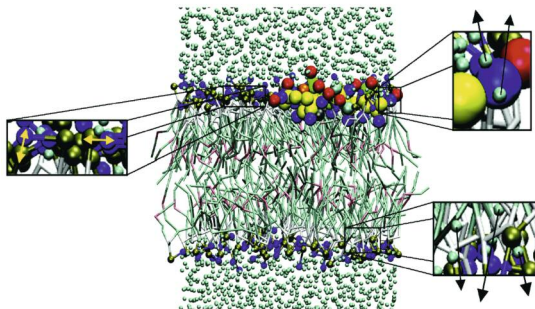


Fig. 2: Configuration of antimicrobial peptide NK-2 (large spheres) at a POPE bilayer from an MD simulation using a coarse grained model [5]. The main contributions to the favorable transfer of NK-2 from POPE to POPC are highlighted; these are a removal of water particles from the hydrophobic core and the nonpolar side chains and an increase in the number of interlipid salt bridges.

Molecular Motors – Force Generators of the Cell

Kinesin motors use the chemical energy supplied by ATP hydrolysis to transport cargo along microtubules (MTs). Because of the ATP hydrolysis, the motor assumes different nucleotide states during its processive motion. These three states differ in their affinities to the microtubule; strong binding of the motor domain to tubulin is observed when the nucleotide-binding pocket is empty or contains ATP whereas weak binding, leading to detachment, occurs when ADP is bound. The catalytic cycle of the motor domains is out-of-phase which facilitates kinesin's walk along the MT. Phosphate release is believed to trigger conformational changes in the motor head leading to detachment of the head from the MT and the undocking of the neck linker from the motor domain. The neck linker is a 10 amino acid residue peptide at the carboxy terminal of the motor domain and, because of its nucleotide dependent flexibility, is proposed to generate a force that brings the trailing motor head to the leading position.

Our simulations of a kinesin head attached to tubulin provide strong evidence for a specific allosteric coupling mechanism that consists of several subsequent molecular transitions which finally lead to the detachment of the neck linker from the motor domain [7]. The initial steps in this cas-

cade of conformational changes induced by phosphate release are indicated in Fig. 3. Interestingly, our simulations reveal conformational changes of the proteins that are quite different from rigid-body transformations as previously assumed when high-resolution X-ray structures were fitted into low-resolution cryo electron microscopy images. In running projects we study the free energy differences between the different nucleotide states assuming a local equilibrium for pairs of states. As the motor energetics depend on the equilibrium constant for the hydrolysis reaction which we would like to understand from ab initio calculations, we are currently testing quantum mechanical methods, starting with the calculation of free energies of formation for gas phase reactions of small molecules. Finally, we investigate the mechanical step itself in full atomic detail with explicit solvent.

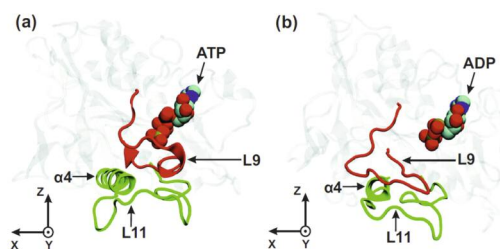


Fig. 3: Dominant conformations of the loops L9 (red) and L11 (green) for kinesin KIF1A attached to tubulin with (a) ATP and (b) ADP in the binding pocket, as obtained from MD simulations [7].

V. Knecht, N. Awasthi, Y. Chai, C v. Deuster, P. Kar, M. Kittner, A. Krukau, T. Pobandt
vknecht@mpikg.mpg.de

References:

- [1] Volker Knecht: Model amyloid peptide B18 monomer and dimer studied by replica exchange molecular dynamics simulations. *J. Phys. Chem. B* **114**, 12701–12707, 2010.
- [2] Madeleine Kittner, Volker Knecht: Disordered versus fibril-like amyloid β (25–35) dimers in water: structure and thermodynamics. *J. Phys. Chem. B*, 2010, **114**, 15288.
- [3] Madeleine Kittner, Alan Mark, Volker Knecht: Structure of Amyloid β (10-35) dimers in water. In preparation.
- [4] Volker Knecht, Annabel Muentert-Edwards, Hans Börner, Gerald Brezesinski: Peptide monolayer with β -sheet structure at water-air interface probed by experiment and simulation. In preparation.
- [5] Carola von Deuster, Reinhard Lipowsky, Volker Knecht: Specificity in binding of antimicrobial peptide to bacterial-like membrane based on hydrophobic effect and intramembrane electrostatics. Submitted.
- [6] Parimal Kar, Reinhard Lipowsky, Volker Knecht: Importance of polar solvation for cross-reactivity of antibody and its variants with steroids. Submitted.
- [7] Aliaksei Krukau, Volker Knecht, Reinhard Lipowsky: Conformational changes of ATP hydrolyzing enzymes from atomistic simulations: Kinesin's motor domain as a case study. Submitted.

Discrete Energy Landscapes of Proteins



Continuous Versus Discrete Energy Landscape

A central goal in protein science is to characterize the free-energy landscapes of folding and binding. Such landscapes result from assigning free energies to all relevant conformations of a protein in a folding or binding process. If the conformations of a protein are described by the Cartesian coordinates of all its atoms, or by internal rotational degrees of freedom, the resulting free-energy landscapes are continuous and high-dimensional. These high-dimensional continuous landscapes have helped to understand general aspects of protein folding and binding (see **Fig. 1**). However, because of their complexity, they are difficult to apply in practice, i.e. to particular proteins or processes. Practical applications of continuous landscapes usually require projections on one or two 'reaction coordinates'. But the choice of such reaction coordinates is often arbitrary, and the projections may hide important aspects of the folding or binding dynamics.

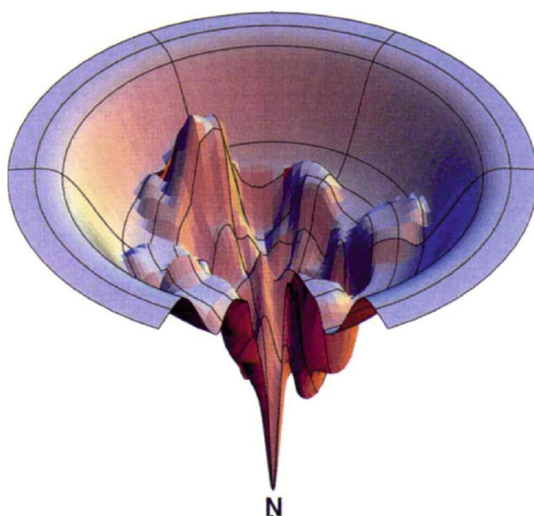


*Fig. 1: Three-dimensional cartoon of a high-dimensional, continuous free-energy landscape of protein folding. The folded, 'native' state N of the protein corresponds to the global minimum on this landscape (from Dill, K. A. and Chan, H. S., *Nat. Struct. Biol.* 4, 10 (1997)).*

To overcome these inherent problems of continuous free-energy landscapes, we have explored discrete landscapes of protein folding and binding in the past years **[1,2,3,4]**. A particularly promising approach is to construct detailed, discrete free-energy landscapes from simulation trajectories **[1]**. The discrete landscapes assign free energies and transition probabilities to a large but finite number of conformational states. These landscapes constitute detailed Markov models of folding or binding.

Discrete Landscapes from Molecular Simulations

Characterizing the equilibrium ensemble of folding pathways is one of the main challenges in protein folding. In principle, this ensemble of pathways is accessible via all-atom molecular dynamics simulations. But in practice, the ensemble is difficult to compute since the affordable simulation times are typically not sufficient to observe a significant number of folding events, unless largely simplified protein models are used. We have suggested a novel approach that allows to reconstruct the ensemble of folding pathways from simulations that are much shorter than the folding time **[1]**. This approach is based on (1) partitioning the state space into small conformational states, (2) constructing a discrete energy landscape, or Markov model, and (3) identifying transition pathways from the unfolded to the folded conformational states.

The first step in this approach involves a clustering of all conformations along the simulation trajectories into typically thousands of conformational states. In the second step, the transition probabilities between these conformational states are estimated from the numbers of transitions observed on the trajectories within a reasonably chosen 'lag time' Δt . The conformational states and transition probabilities represent a discrete landscape, or Markov model, of the folding process.

We have applied this approach to a set of 180 atomistic molecular dynamics trajectories of the Pin WW domain in explicit solvent **[1]**. The length of each of these trajectories is about two orders of magnitude shorter than the folding time of this protein. However, by jointly analysing these 180 trajectories, which 'explore' different regions of the energy landscapes, the folding pathways can be reconstructed, despite the fact that no contiguous pathway from the unfolded to the folded state is observed in a single simulation.

Thomas Weikl 01.04.1970

1996: Diploma, Physics

(Freie Universität Berlin)

Thesis: Interactions of rigid membrane inclusions

1999: PhD, Physics

(Max Planck Institute of Colloids and Interfaces, Potsdam)

Thesis: Adhesion of multicomponent membranes

2000-2002: Postdoc

(University of California, San Francisco)

Since 2002: Group Leader

(Max Planck Institute of Colloids and Interfaces, Potsdam)

2008: Habilitation, Physics

(University Potsdam)

Thesis: Transition states and loop-closure principles in protein folding

Folding Pathways and Folding Flux

To characterize the folding pathways in the third step of our approach, we have to identify conformational states on the energy landscape that correspond to the folded and the unfolded state of the protein. All remaining conformational states on the landscape are partially folded, intermediate states. The central quantity to characterize the folding pathways is the folding probability of these intermediate states. The folding probability of an intermediate state is the probability for reaching the folding state prior to the unfolded

state. This folding probability, or 'committor', defines a direction on the energy landscape along which the folding flux between pairs of states can be computed. In a coarse-grained representation, the resulting folding flux for the PIN WW domain is depicted in Fig. 2. An interesting aspect of the PIN WW folding dynamics are metastable 'traps' in which the two β -hairpins of this protein are incorrectly folded.

T. Weikl, L. Reich
thomas.weikl@mpikg.mpg.de

References:

- [1] Noe, F., Schütte, C., Vanden-Eijnden, E., Reich, L. and Weikl, T. R.: Constructing the equilibrium ensemble of folding pathways from short off-equilibrium simulations. *Proc. Natl. Acad. Sci. USA* **106**, 19011-19016 (2009).
Commentary: Gruebele, M.: How to mark off paths on the protein energy landscape. *Proc. Natl. Acad. Sci. USA* **106**, 18879-18880 (2009).
- [2] Weikl, T. R. and von Deuster, C.: Selected-fit versus induced-fit protein binding: Kinetic differences and mutational analysis. *Proteins* **75**, 104-110 (2009).
- [3] Reich, L., Becker, M., Seckler, R. and Weikl, T. R.: In vivo folding efficiencies for mutants of the P22 tailspike-helix protein correlate with predicted stability changes. *Biophys. Chem.* **141**, 186-192 (2009).
- [4] Weikl, T. R.: Transition states in protein folding. *Commun. Comput. Phys.* **7**, 283-300 (2010).

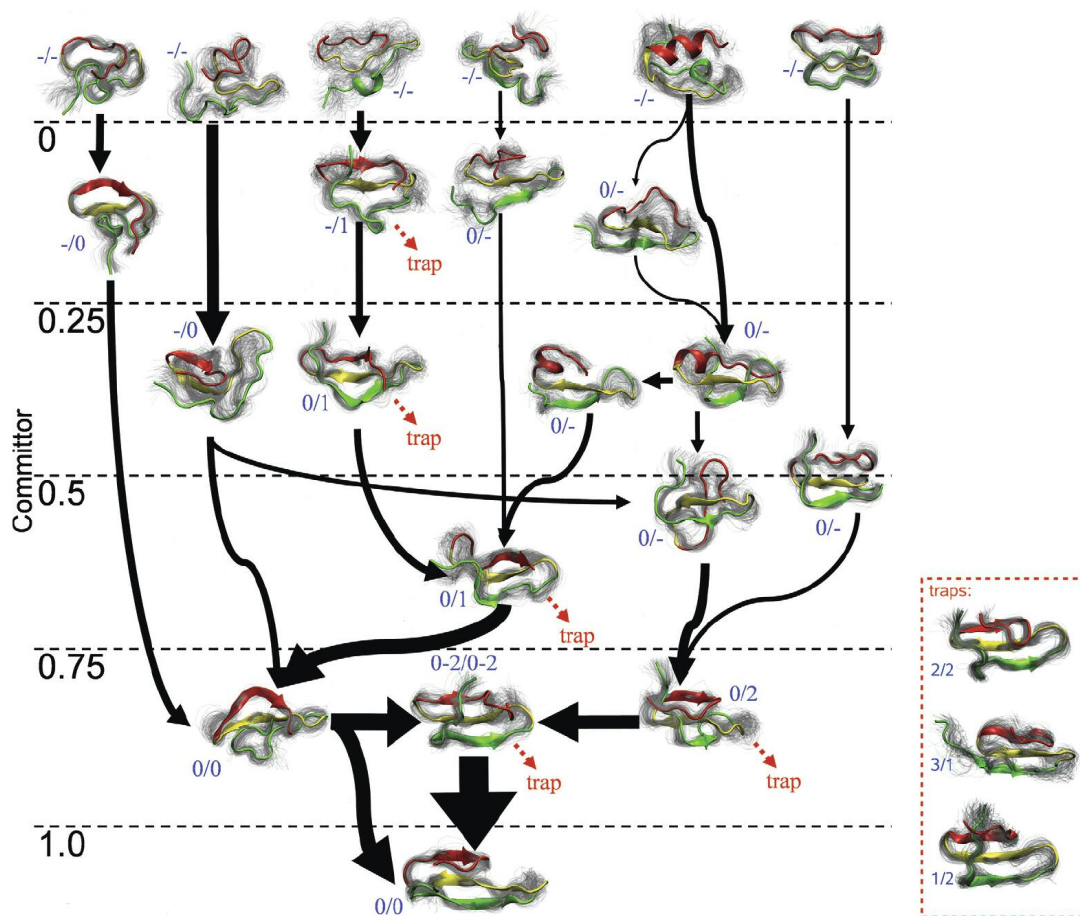


Fig. 2: Discrete landscape for the folding of the PIN WW domain. The folded structure (bottom) of this protein consists of two β -hairpins that form a three-stranded β -sheet. In this diagram, the unfolded state of the protein is represented by six conformational states (top). The numbers on the left indicate the committor probability, or folding probability, of each state. For each conformational state, a representative mean structure is shown in color, along with an overlay of equilibrium-distributed structures in this state to indicate the structural flexibility (gray cloud). The black arrows represent the probability flux between the states in folding direction. Besides 'correct' hydrogen bond alignments, or 'registers', in the two hairpins, we observe also conformational states in which these hydrogen bond registers are shifted by one or two residues compared to the folded state. The blue numbers next to the structures indicate whether the first/second hairpin has the native register (0), is register-shifted by one or two residues (1,2) or is not formed at all (-). Some of these register-shifted states are 'traps' without significant folding flux (lower right).

Nanoparticles and Polymer Brushes



Christian Seidel 07.02.1949

1972: Diploma, Physics

(Technical University Dresden)

Thesis: Calculation of angular distribution and polarization of nucleon scattering close to resonance energies

1978: Dr. rer. nat., Polymer Physics

(Institute for Polymer Chemistry,

Teltow) Thesis: On the calculation

of the phonon dispersion of solid

polymers, application to

polyvinylidenefluoride

1979-83: Research Scientist

(Ioffe Physico-Technical

Institute, Leningrad)

1983-89: Research Scientist

(Institute for Polymer

Chemistry, Teltow)

1985: Dr. sc. nat.,

Solid State Theory (Institute for

Polymer Chemistry, Teltow)

Thesis: Ground states and critical

temperatures in quasi-one-dimensional

systems

1989-91: Group Leader

(Institute for Polymer Chemistry, Teltow)

Since 1992: Group Leader

(Max Planck Institute of Colloids

and Interfaces, Potsdam)

1994: Habilitation,

Theoretical Chemistry

(Technical University, Berlin)

Polymer brushes, i.e. polymers densely anchored to an interface have received much interest because of their scientific and technological importance. In good solvents the polymers are stretched away from the grafting plane causing a steep density gradient at the rim of the brush. Brushes consisting of two or more incompatible components are of special interest because they exhibit phase separation on nanometer scales. Morphological transitions and microphase separation are driven by immiscibility and/or contrast in solvent affinity. Lateral segregation can lead to stable surface nanopatterns and enables surface tuning as well as "smart" surfaces that respond to some extent to external stimuli. One of the less understood and still challenging problems in polymer science is the behavior of hybrid systems composed of polymer brushes and nanoparticles. On the one hand, even a small amount of such additives may have strong effects on the brush layer. On the other hand polymer brushes can be used to control the organization of nanoparticles into larger aggregates. We use dissipative particle dynamics (DPD) simulations that models molecules in solution on a coarse-grained level [1] to study both the morphology of heteropolymer brushes and the organization of nanoparticles guided by polymer brushes. In our model, there are five different types of DPD beads: polymer A and B blocks (A, B), solvent (S), nanoparticles (P), and wall (W).

Nanoparticles at Homopolymer Brushes

In this situation, the polymer brush consists of solvophilic A blocks only. Polymer-insoluble nanoparticles immersed into the brush are treated as rather rigid aggregates composed of 9 DPD beads, which are interconnected by harmonic springs. They exhibit an almost spherical form. To minimize the penalty in surface energy they tend to aggregate. Exceeding a certain size these aggregates are expelled towards the brush-solvent interface. The equilibrium state depends on the polymer-nanoparticle-solvent interfacial tensions γ_{AS} , γ_{AP} , γ_{PS} . The DPD interaction parameters can be chosen such that the spreading coefficient $S = \gamma_{AS} - \gamma_{AP} - \gamma_{PS}$ is negative, i.e., nanoparticles do not wet the brush surface, while the entry coefficient $E = \gamma_{AS} + \gamma_{AP} - \gamma_{PS}$ is positive, i.e. nanoparticles are drawn into the polymer film. Under such conditions, theory predicts nanoaggregates that grow freely in one lateral direction only. In the second direction, the supporting brush restricts growth. Varying nanoparticle concentration ϕ , in nice agreement with the prediction, we find a crossover from a vertical cylinder shape at small ϕ over a horizontally oriented flattened sphere to a highly anisotropic baguette-like shape at large ϕ (see Fig. 1) [2].

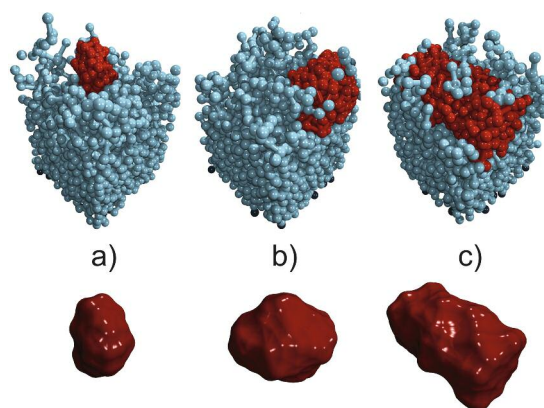


Fig. 1: Nanodroplets in the distal brush region at growing nanoparticle concentration ϕ (from left to right). Polymer beads are colored blue and nanoparticle ones red. Solvent beads are hidden. Bottom part: Connolly surfaces of the nanodroplets.

Surface Pattern of Diblock Copolymer Brushes

While macroscopic surface properties such as wettability and adhesion only depend on the average composition of the top layer on large length scales, the interaction of brushes on nanoscales is governed by the details of its morphology. To make substantial progress with applications based on polymer pattern on nanoscales, a detailed understanding of the microphase separation in multiblock brushes is of fundamental importance. We study tethered diblock copolymers in selective solvents where the chains are anchored via the ends of soluble A blocks while the solvent is poor for B blocks. Under such conditions, A blocks form stretched brushes whereas insoluble B blocks exhibit different morphologies, which depend both on solvent quality $\tau_B = a_{BS}/a_{BS}^{(0)} - 1$, where a_{BS} is the DPD parameter setting the repulsion between B blocks and solvent, and on chain composition $\square_B = N_B / (N_A + N_B)$, where $N_{A,B}$ are the lengths of A and B blocks, respectively. Fig. 2 gives the morphology diagram in the $\square_B - a_{BS}$ parameter space studied by simulations and Fig. 3 shows typical simulation snapshots [3]. With increasing length of B blocks, in the top brush layer we obtain transitions from spherical B micelles (hexagonal phase) via cylindrical micelles (stripes) and spherical A micelles (inverted hexagonal) to a uniform lamella. This observation is in agreement with experimental findings. Note that we treat A-B incompatibility and solvent selectivity separately by two independent parameters a_{AB} and a_{BS} . Analyzing the micellar aggregates we found an unusual feature not obtained in previous one-parameter models. In Fig. 4, the average number of chains per spherical micelle is plotted as a function of solvent quality. Obviously it saturates at large τ_B or $a_{BS} > a_{AB}$. Supported by simulation snapshots this behavior indicates that the solvophobic B domains are covered by soluble A blocks to reduce unfavorable interactions with solvent.

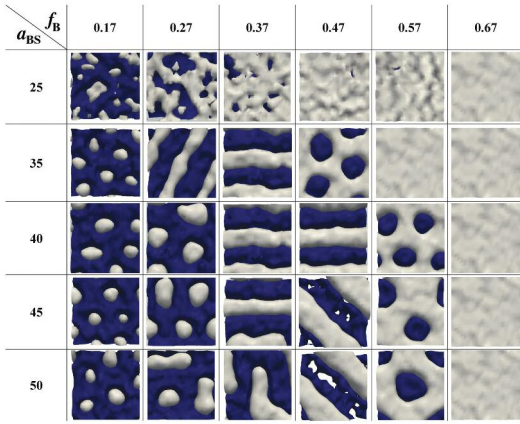


Fig. 2: Morphology diagram of diblock copolymer brushes in selective solvents in terms of polymer composition f_B and solvent quality (interaction parameter α_{BS}). Shown is the top view of equidensity plots where A and B regions are colored dark and light grey, respectively.

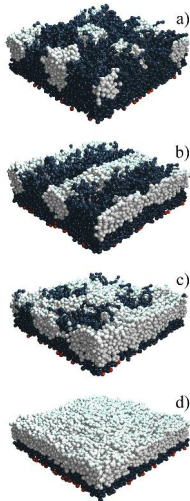


Fig. 3: Typical morphologies obtained at $\alpha_{BS}=40$ and varying polymer composition: a) $f_B=0.17$, b) 0.37 , c) 0.57 , and d) 0.67 . Coloring similar to Fig. 2.

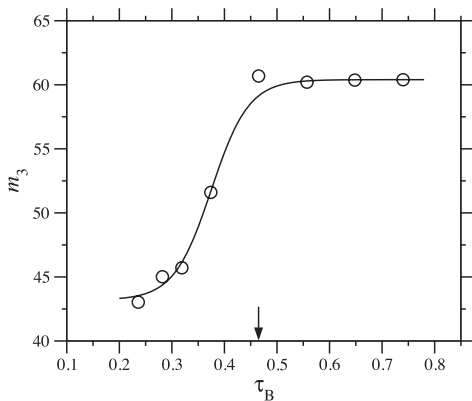


Fig. 4: Average number of chains per micelle versus solvent quality. The arrow indicates τ_B where α_{BS} equals α_{AB} . At $\alpha_{BS} > \alpha_{AB}$ the behavior becomes independent of solvent quality (see text).

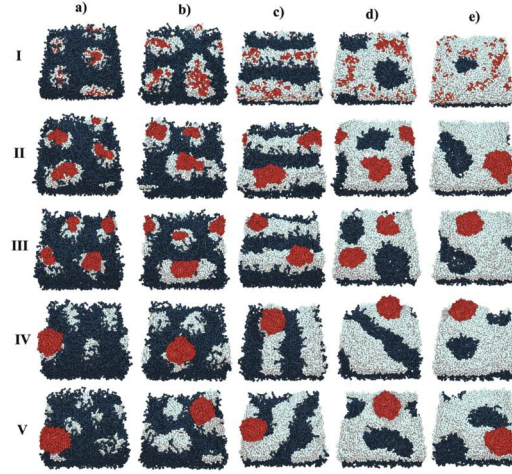


Fig. 5: Nanocomposite systems of diblock copolymer brushes and nanoparticles at different polymer composition with f_B growing from left to right and variable interaction strength between nanoparticles and B blocks with α_{BP} growing from top to down.

Diblock Copolymers as Template for Nanoparticles

Beside the uninteresting laterally homogeneous lamella phase the morphology diagram shown in Fig. 2 exhibits two major pattern types that can be used to establish templates for the organization of nanoparticles: (i) hexagonally packed dots and (ii) periodic line pattern. Fig. 5 shows a typical brush-nanoparticle pattern diagram in the $f_B - \alpha_{BP}$ space [4]. The constant parameters are $a_{AB}=a_{BS}=a_{PS}=a_{AP}=40$, $a_{AS}=25$, $\phi=0.112$. For $\alpha_{BP}=25$ (row I), nanoparticles are soluble in B domains and aggregate inside those domains following their shape. In this case nanoparticles increase the effective B block fraction, which causes a corresponding shift in the morphology diagram of the underlying brush. For moderate α_{BP} (rows II, III), we obtain finite spreading of nanoparticle droplets along B regions. In the situation shown in Fig. 5, spreading is restricted because of the large surface tension due to $a_{PS}=40$. For large $\alpha_{BP}>40$ (rows IV, V), nanoparticles form a single droplet on the top of a B domain. Fig. 5 illustrates the complex challenge to use diblock copolymer brushes as soft templates for nanoparticle organization. However, numerical simulations offer a powerful tool to detect and to analyze the most interesting regions of the huge parameter space.

C. Seidel, O. A. Guskova, and S. Pal*)
seidel@mpikg.mpg.de.

*) present address: Evotec Ltd, Abingdon, UK

References:

- [1] Pal, S., Seidel, C.: Dissipative Particle Simulations of Polymer Brushes: Comparison with Molecular Dynamics Simulations. *Macromol. Theory Simul.* **15**, 668 (2006).
- [2] Guskova, O. A., Pal, S., Seidel, C.: Organization of Nanoparticles at the Polymer Brush-Solvent Interface. *EPL.* **88**, 38006 (2009).
- [3] Guskova, O. A., Seidel, C.: Mesoscopic Simulations of Morphological Transitions of Stimuli-Responsive Diblock Copolymer Brushes. *Macromolecules*, to be published (2011).
- [4] Guskova, O. A., Seidel, C.: in preparation.

Conformational Dynamics of Complex Oligosaccharides



The operation and stability of many types of biomolecules in the extracellular matrix are influenced by the presence of attached carbohydrate residues. The specific function of these sugar components and thus their potential, e.g., for developing novel vaccines, are to a large extent unknown.

Systematic exploration of *glycans* is difficult in general. Experimental access is mostly limited to solution NMR, and on the numerical side, the abundance of different types of glycosidic linkages inhibits the development of generalizable force fields suited for molecular dynamics (MD) simulations.

In this situation, *invariant* carbohydrate components may serve as a starting point for a more concise investigation. The backbone of the so-called Glycosylphosphatidylinositol (GPI) anchor that covalently binds many types of proteins to cell membranes, is an example of such a recurrent core structure.

Atomistic Modelling of the GPI backbone

The whole molecule linking a protein to the cell membrane consists of several parts, see **Fig. 1**. An ethanolamine residue links the protein to a backbone carbohydrate sequence which connects via an inositol ring and a phosphate group to a fatty acid immersed in a cell membrane **[1]**. The whole GPI anchor is expressed in a large number of variations, phosphate groups and/or further oligosaccharides being attached to the hydroxyl groups of the backbone. A prototypical question to ask here is: what kind of characteristic overall structure does the backbone maintain?

To model the backbone atomistically, we employ an all-atom bio-molecular force field particularly devoted to carbohydrates **[2]**. It is also sufficiently generalizable to adopt a strategy of independently considering various fragments of the backbone. This facilitates comparison with detailed NMR studies (2D-NOE spectra of di- and tri-saccharide fragments) and also allows us to run long simulation trajectories on a single fragment: conformational dynamics significantly slows down because of the surrounding aqueous solution which must be modeled explicitly, since many hydroxyl groups maintain a complicated network of hydrogen bonds with solvent water molecules.

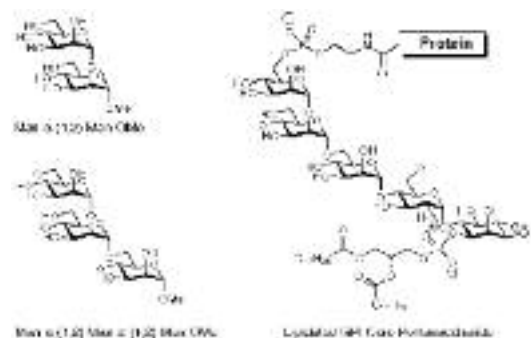


Fig. 1. GPI-core structure in its simplest configuration (right). The backbone consists of 4 sugars and one inositol ring. For detailed experimental (NMR) and theoretical (MD) analysis, the backbone can be decomposed into adequate subunits, two of which are to the left. The chemical structure formulas only indicate the molecule topology, not the actual geometric conformation.

Dynamics of Glycosidic Linkages

Because single sugar rings are relatively rigid, the conformational preferences of an oligosaccharide can be characterized in much the same way as torsion angles within a peptide backbone. In **Fig. 2**, the disaccharide 1-6-linkage, central to the backbone, is shown. The overall dihedral dynamics is revealed only with long (100ns-1 μ s) MD-simulations. The glycosidic angle trajectories reveal the different time scales involved. Whereas during periods up to several tenths of nanoseconds a conformation corresponding to one particular value of omega may appear very stable, on a time scale one order of magnitude larger the picture changes completely. On yet larger timescales, the molecule thus appears quite flexible. For the backbone, it might even turn out that it can rather be viewed as a flexible chord, particular conformational preferences losing their significance **[3]**.

Mark Santer 27.10.1971

2003: PhD in Physics at the University of Freiburg

2003-2006: Postdoc at the Institute of Microsystems Engineering, University of Freiburg. Group leader Nanofluidics

2006-2009: Employee at the Fraunhofer Institute of Mechanics of Materials (IWM), Freiburg

2009: 2010 Postdoc at the Theory Department, MPI for Colloids and Interfaces, Potsdam

From 09/2010: Group leader Carbohydrates and Polysaccharides at Theory Department

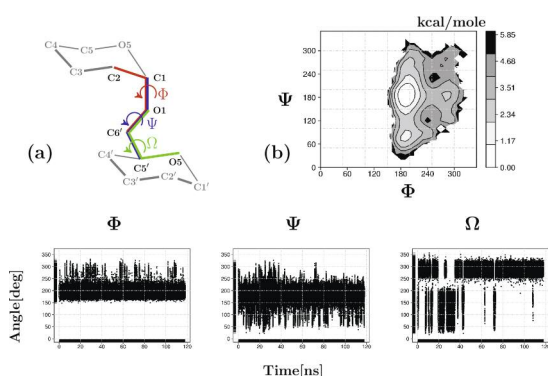


Fig. 2. (a) Definitions of dihedral angles for a 1-6 linkage between two mannoses (exocyclic groups omitted). Lower ring is the reducing end (primed). (b) Frequency distribution of Phi-Psi occurrences, converted to energy units (histogram assembled from 240.000 data points during a 120ns simulation). Lower panel: trajectories of the three glycosidic dihedral angles taken from the same simulation run.

Characterising Oligosaccharides on a Monomer Basis

Complementary to a “per linkage” point of view is to consider the oligosaccharide on a “per monomer” basis. One may ask which properties of a monosaccharide unit, apart from possible linkages to others, may favor its occurrence in a certain oligosaccharide. To tackle this question one may simply start with looking at differences across a stereo-chemical series. For a certain subset of aldohexoses the chemical formula is the same, yet they differ in orientation of their hydroxyl groups. In a preliminary studies we are considering mannose and glucose, deviating only in the orientation of their hydroxyl group at the C2 carbon atom. Within our atomistic model, we have used thermodynamic integration to grow glucose into mannose in solution as well as in vacuum, the differences of these values determining the variation in solvation free energy between the two molecules [4]. Especially in vacuum the analysis is complicated by the trapping of hydroxyl and hydroxy-methyl conformations, resulting in large and strongly varying error bars, see Fig. 3. No standard procedure is available to meet this situation. In our case one has to force the molecule to go along a smoother path between the initial and final state, a procedure that finally leads to a respectable difference of 1.8 kcal/mole between the two species.

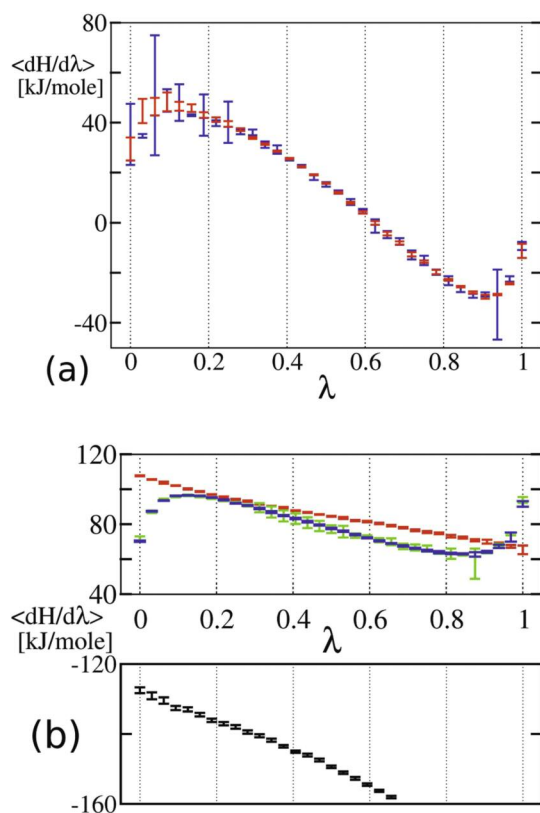


Fig. 3. Behavior of the derivative of the internal energy $\langle H(\lambda) \rangle$ with respect to the thermodynamic integration parameter λ , for two distinct paths leading from Glucose ($\lambda=0$) to Mannose ($\lambda=1$) in vacuum. (a) all parts of the molecular Hamiltonian vary simultaneously (blue: 1.6ns simulation time per data point, red: 16ns). (b) Before changing the molecular topology, charges on hydroxyl hydrogens are absorbed into their oxygen atoms (red). At least for the simulations with 16ns per data point (blue), we can achieve a smooth variation with relatively small error bars. The lower panel in (b) shows the contribution to the free energy change, when all remaining charges are restored (last part of the graph omitted for clarity).

The general type of difficulty met here is similar to the dynamical study of the backbone. Averages of any kind of observables are strongly influenced by a series of closely spaced conformers.

M. Santer, M. Wehle and R. Lipowsky,
mark.santer@mpikg.mpg.de

References:

- [1] A. Varki et al., Essentials of Glycobiology. CSH Press, Cold Spring Harbor NY
- [2] K. Kirschner et al., J. Comp. Chem. **29**, pp. 622 (2007)
- [3] Wehle, M., Lipowsky, R. and Santer, M.: Challenges in simulation studies of oligosaccharides. Is the GPI-backbone a hinge or a chord? In preparation
- [4] M. Santer and R. Lipowsky: Influence of Stereochemistry on the Solvation Free Energy of Aldoses. A Molecular Dynamics study. In preparation

Membranes, Ions, and Water at the Molecular Level



The function of biomembranes is not restricted to surrounding a cell and its various compartments as inert separation layers. By facilitating transport of molecules from one side to the other, they play also an active role. Membranes are composed of a complex mixture of various lipids and proteins, with the lipids forming a bilayer. Our aim is to understand biomembranes in terms of the self-organization of

these constituents. The experimentally accessible information about the molecular architecture of membranes is very limited. Therefore, we use molecular dynamics simulation techniques to study the cooperative processes underlying the mesoscopic properties of membranes. As a first step, we model membranes as lipid bilayers.

Membranes and Ions

A biomembrane *in vivo* is surrounded by an aqueous solution containing ions. The most abundant atomic monovalent ions are potassium (K^+), sodium (Na^+), and chloride (Cl^-). Sodium and potassium can be specifically adsorbed at membranes as indicated from various experimental and simulation studies, the membrane affinity being somewhat higher for Na^+ than for K^+ . In order to model interactions of ions with a membrane, a reliable force field is required but a force field for K^+ in conjunction with the widely used simple point charge (SPC) model for water has not been available.

We have derived a force field for K^+ matching activity coefficients of aqueous KCl solutions for a wide range of concentrations, as shown in Fig. 1 [1]. The figure also shows that the solution activities of other force fields significantly deviate from the experimental values. Our force field for KCl is shown to also reproduce the experimental binding constant for the adsorption of K^+ at a POPC bilayer as shown in Fig. 2 [2, 3].

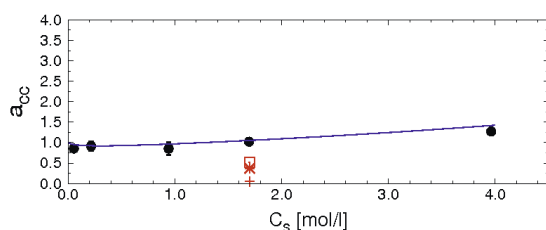


Fig. 1: Activity derivative of aqueous KCl solutions as a function of the molar KCl concentration [1]. The line shows a fit to the experimental data, the black circles indicate the results for our KCl force field with simple point charge (SPC) water, and the red symbols show the results for force fields from the literature.

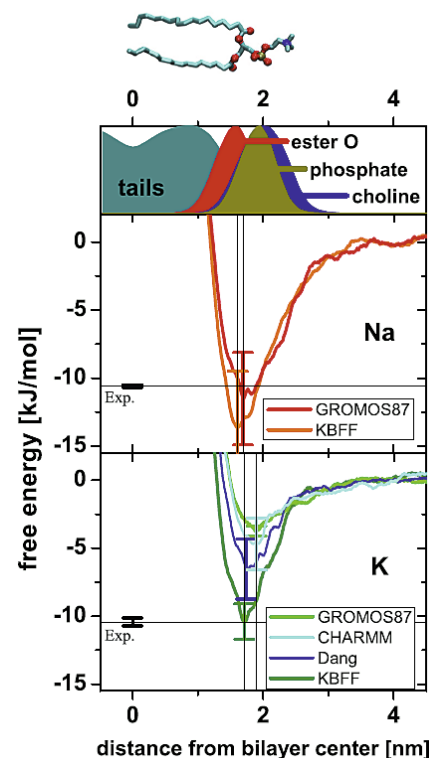


Fig. 2: Free energy as a function of the distance of sodium or potassium from the center of a POPC bilayer for different ion force fields [2]. The horizontal lines show the experimental adsorption free energies (Exp.) [3] for the respective cation chloride. The distribution of various atomic groups normal to the bilayer and a representative lipid configuration are shown as a reference.

In contrast, models used in previous simulation studies are found to underestimate the membrane affinity of K^+ , thus exaggerating the difference between Na^+ and K^+ . Our simulations support the view that ion adsorption at PC membranes is driven by an entropy gain due to the release of hydration water from the ions and the lipids.

The interaction of ions with membranes also affects the tendency of membranes to fuse with one another, a key step in intracellular traffic, viral infection, and liposome-mediated drug delivery. The latter is achieved by pH-responsive liposomes. One important component of such systems is cholesterol hemisuccinate (CHEMS) being negatively charged and forming stable liposomes above pH 6 and being neutral below pH 5 where it becomes fusogenic. Our MD simulations explain this behavior showing strong binding of counterions to anionic CHEMS and counterion release for neutral CHEMS

Volker Knecht 06.01.1970

1996: Diploma in Physics

(University of Kaiserslautern)

Thesis: Computer based renormalization group study of the two-dimensional XY model

1997: Software trainee

(TECMATH GmbH, Kaiserslautern)

1998-1999: Software engineer

(LMS Durability Technologies GmbH, Kaiserslautern)

2003: PhD, Physics (MPI of biophysical chemistry, Göttingen)

Thesis: Mechanical coupling via the membrane fusion SNARE protein syntaxin 1A: a molecular dynamics study

2003-2005: Postdoc

(University of Groningen,

the Netherlands)

2005-2006: Postdoc

(MPI of Colloids and Interfaces, Potsdam)

Since 2006: Group Leader

(MPI of Colloids and Interfaces, Potsdam)

as shown in **Fig. 3**. Counter ion release is found to correlate with a decrease in the effective headgroup size known to promote fusion [4].

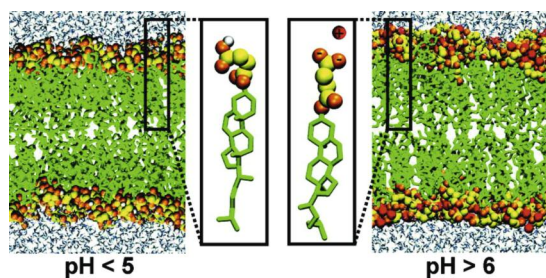


Fig. 3: Cutout cross sections of hydrated CHEMS bilayers in (left) protonated state and (right) deprotonated state with sodium, the insets showing individual CHEMS molecules [4].

Membrane Fusion

The fusion of two membranes requires the approach of the membranes, the latter being hindered by strong repulsive hydration forces. We have computed the hydration forces between two POPC bilayers using a coarse grained model and get good agreement with experimental values. Our results suggest that, unlike suggested previously, the directionality of hydrogen bonds between the lipids and water, not described in our model, is not essential for the occurrence of hydration forces [5].

Once two membranes are close to each other, the hydration forces can be circumvented by the formation of small defects which can lead to the formation of so-called “stalks” between the two bilayers formed by multiple lipids. Our simulations show that such defects are related to the exposure of hydrophobic lipid tails to the water, as shown in **Fig. 4** [6]. Peptides derived from the fusion hemagglutinin fusion protein of the influenza virus and denoted as fusion peptides, known to induce membrane fusion in vitro, do not accelerate stalk formation and even increase the hydration forces, thus not facilitating fusion kinetically. However, they can stabilize stalk-pore complexes thermodynamically as shown by self-assembly, leading to a new, so-called simple cubic phase, induced by the peptides [7]. We do find that fusion peptides strongly stabilize membrane nanopores, in good correlation with experiments. Even in the absence, though, membrane nanopores are kinetically stabilized by a small energy barrier, as we have revealed from atomistic simulations [8].

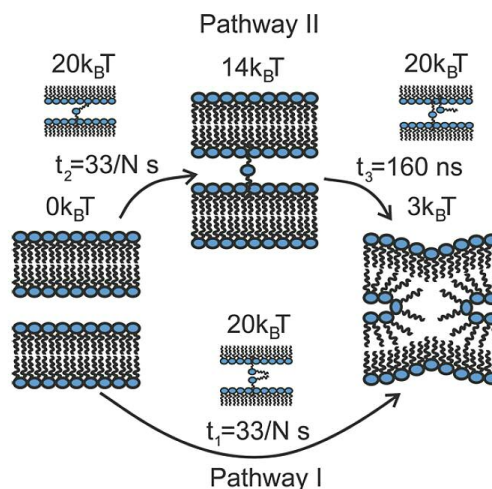


Fig. 4: Early membrane fusion energetics and kinetics for two POPC bilayers separated by five waters per lipid [6]. The symbol N denotes the number of lipids in the proximate leaflets.

Electrokinetic Phenomena

Hydrophobic surfaces in water are widely believed to adsorb hydroxide (OH⁻) ions. This is suggested by the fact that oil droplets in water exposed to an electric field move as if they were negatively charged (i.e., they exhibit negative electrophoretic mobilities). However, we have performed MD simulations using an all-atom polarizable potential reproducing the sign and the size of the electrophoretic mobilities of oil in water although ions were absent, as indicated in **Fig. 5** [9]. The underlying mechanism is related to the polarization of the water and the oil at the interface. Our results may help to resolve a current controversy concerning the charge of hydrophobic surfaces in water. Interestingly, non-classical electrokinetic phenomena - in the form of charge inversion - also occur in biology, playing a role in the function of kidney and related diseases [10].

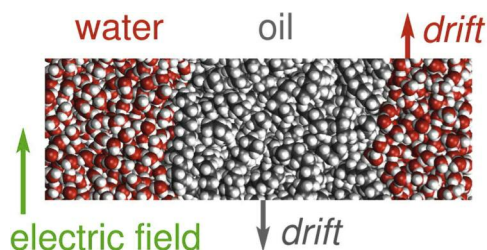


Fig. 5: An electric field applied parallel to a water/oil interface induces a tangential movement between the phases [9]. The effect requires a sufficiently detailed model describing not only the water but also the oil in full atomic detail and using a polarizable interaction potential.

V. Knecht, B. Klasczyk, Y. Smirnowa
vknecht@mpikg.mpg.de

References:

- [1] Benjamin Klasczyk, Volker Knecht: Kirkwood-Buff force field for alkali chlorides in simple point charge water. *J. Chem. Phys.*, **132**, 024109, 2010.
- [2] Benjamin Klasczyk, Volker Knecht: Validating affinities for ion-lipid association from simulations against data from isothermal calorimetry. Submitted.
- [3] Benjamin Klasczyk, Volker Knecht, Reinhard Lipowsky, Rumiana Dimova: Interactions of alkali metal chlorides with phosphatidylcholine vesicles. *Langmuir* **26**, 18951, 2010.
- [4] Benjamin Klasczyk, Steffen Panzner, Reinhard Lipowsky, Volker Knecht: Fusion-relevant changes in lipid shape of hydrated cholesteryl hemisuccinate induced by pH and counterion species. *J. Phys. Chem. B* **114**, 14941, 2010.
- [5] Yuliya G. Smirnova, Siewert-Jan Marrink, Reinhard Lipowsky, Volker Knecht: Hydration forces between phospholipid bilayers from coarse grained molecular dynamics simulations. In preparation.
- [6] Yuliya G. Smirnova, Siewert-Jan Marrink, Reinhard Lipowsky, Volker Knecht: Solvent-exposed tails as pre-stalk transition states for membrane fusion at low hydration. *J. Am. Chem. Soc.* **192**, 6710, 2010.
- [7] M. Fuhrmans, V. Knecht, S.J. Marrink: A single bicontinuous cubic phase induced by fusion peptides. *J. Am. Chem. Soc.* **131**, 9166, 2009.
- [8] Andrea Grafmüller, Reinhard Lipowsky, Volker Knecht: Free energy barrier stabilizing membrane nanopores. Submitted.
- [9] Volker Knecht, Zachary A. Levine, P. Thomas Vernier: Electrophoresis of neutral oil in water. *J. Colloid Interface Science* **352**, 223, 2010, Editor's Choice (Cover Article).
- [10] Ralf Hausmann, Christoph Kuppe, Herbert Egger, Frank Schweda, Volker Knecht, Marlies Elger, Sylvia Menzel, Douglas Somers, Gerald Braun, Astrid Fuss, Sandra Uhlig, Wilhelm Kriz, George Tanner, Jürgen Floege, Marcus J. Moeller: Electrical Forces Determine Glomerular Permeability. *J. Am. Soc. Nephrol.* **21**, 2053-2058, 2010.

MEMBRANES AND VESICLES

Binding Cooperativity of Membrane Adhesion Receptors



Thomas Weikl 01.04.1970

1996: Diploma, Physics

(Freie Universität Berlin)

Thesis: Interactions of rigid

membrane inclusions

1999: PhD, Physics

(Max Planck Institute of Colloids

and Interfaces, Potsdam)

Thesis: Adhesion of

multicomponent membranes

2000-2002: Postdoc

(University of California,

San Francisco)

Since 2002: Group Leader

(Max Planck Institute of Colloids

and Interfaces, Potsdam)

2008: Habilitation, Physics

(University Potsdam)

Thesis: Transition states and loop-

closure principles in protein folding

Cell adhesion processes are essential for the distinction of self and foreign in immune responses, the formation of tissues, or the signal transduction across the synaptic cleft of neurons. The adhesion processes are mediated by the specific binding of receptor and ligand proteins anchored in the cell membranes. Because of the importance of these processes, the binding of cells to other cells or to surface-supported lipid membranes with anchored ligand molecules (see Fig. 1) has been studied intensively.

Binding Affinity of Receptors and Ligands

A central question is how to characterize and measure the binding affinity of the membrane-anchored receptor and ligand molecules that are involved in cell adhesion. For *soluble* receptor and ligand molecules, the binding affinity can be characterized by the binding equilibrium constant K_{3D} , defined by

$$[RL]_{3D} = K_{3D}[R]_{3D}[L]_{3D} \quad (1)$$

where $[RL]_{3D}$ is the volume concentration of bound receptor-ligand complexes, and $[R]_{3D}$ and $[L]_{3D}$ are the volume concentrations of unbound receptors and unbound ligands in the solution. The equilibrium constant K_{3D} is determined by the binding free energy of the complex and can be measured with standard experimental methods.

An often considered two-dimensional analogue for *membrane-anchored* receptors and ligands is the quantity

$$K_{2D} = \frac{[RL]}{[R][L]} \quad (2)$$

where $[RL]$, $[R]$, and $[L]$ are the *area* concentrations of bound receptor-ligand complexes, unbound receptors, and unbound ligands. However, different experimental methods to measure K_{2D} lead to values that differ by several orders of magnitude, which indicates that K_{2D} is not a proper constant [1].

Membrane Fraction within Receptor Binding Range

Quantifying the affinity of membrane-anchored receptor and ligand molecules is complicated by the fact that the binding process depends on the local separation and, thus, the conformations of the two apposing membranes. A receptor molecule can only bind an apposing ligand if the local membrane separation is comparable to the length of the receptor-ligand complex. A central quantity therefore is the fraction P_b of the apposing membranes with a separation within the binding range of the receptor-ligand interaction. The concentration of bound receptor-ligand complexes

$$[RL] = P_b K_b [R][L] \quad (3)$$

is proportional to P_b , as well as to the concentrations $[R]$ and $[L]$ of unbound receptors and ligands [1,2,4]. Here, K_b is the well-defined two-dimensional equilibrium constant for membrane segments within the binding range of the receptors and ligands.

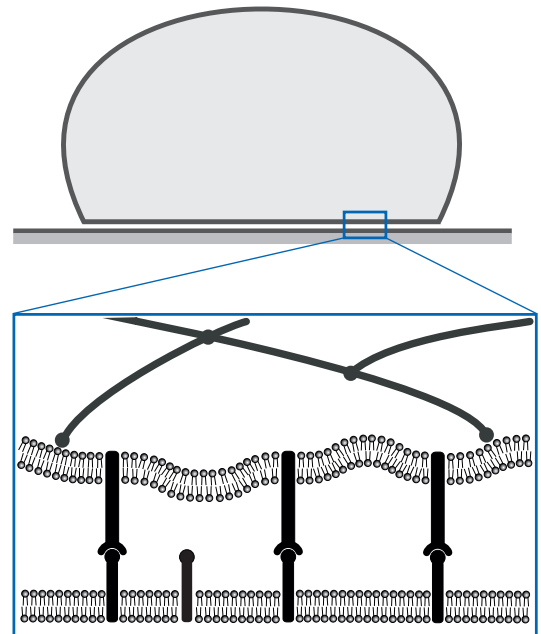


Fig. 1: A cell adhering to a supported membrane with anchored ligands that bind to receptors in the cell membrane. The binding of receptors and ligands in the cell adhesion zone is affected by membrane shape deformations and fluctuations on nanometer scales, which are dominated by the bending rigidity of the cell membrane. The adhesion receptors of immune cells are typically mobile along the membrane only weakly, coupled to the cytoskeleton, if at all.

Thermal shape fluctuations of the membranes on nanometer scales lead in general to values of P_b smaller than 1. For cell membranes, these nanometer scale fluctuations are not, or only weakly, suppressed by the cell cytoskeleton, in contrast to large-scale shape fluctuations.

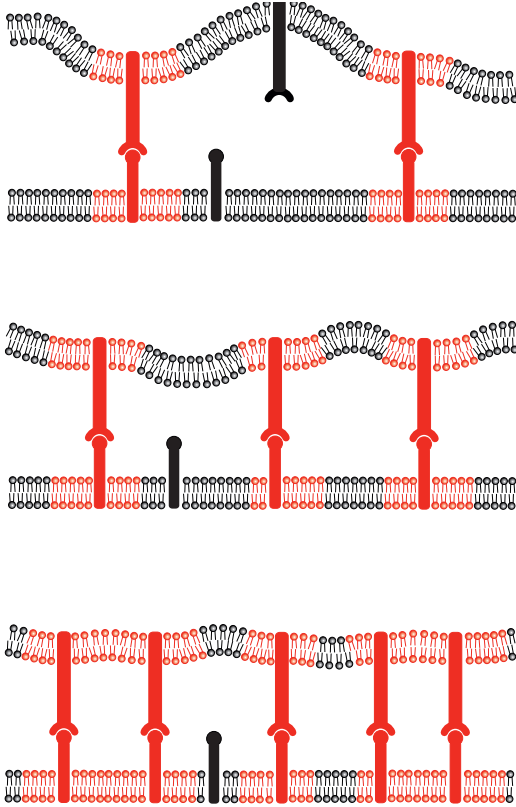


Fig. 2.: An important quantity is the area fraction P_b of the membranes within binding separation of the receptors and ligands. The area fraction P_b (shown in red) increases with the concentrations of receptors and ligands, since the formation of receptor-ligand bonds ‘smoothens out’ thermal membrane shape fluctuations. The ‘smoothing’ facilitates the formation of additional receptor-ligand bonds and, thus, leads to a binding cooperativity [1,2,4].

We have developed a statistical-mechanical model of membrane adhesion in which the membranes are described as discretized elastic surfaces and the adhesion receptors and ligands as individual molecules diffusing on these surfaces [2]. In our model, the fraction P_b of the membranes within binding range of the receptors and ligands turns out to be much smaller than 1 for typical lengths and concentrations of receptors and ligands in cell adhesion zones. Scaling analysis and Monte Carlo simulations lead to the relation

$$P_b \approx c(\kappa/k_B T) l_{we}^2 K_b [R][L] \quad (4)$$

which indicates that the membrane fraction P_b within the binding range of the receptors and ligands is proportional to $[R]$ and $[L]$. Here, $c \approx 13$ is a dimensionless prefactor, $\kappa = \kappa_1 \kappa_2 / (\kappa_1 + \kappa_2)$ is the effective bending rigidity of the two opposing membranes with rigidities κ_1 and κ_2 , $k_B T$ is Boltzmann’s constant times temperature, and l_{we} is the interaction range of the receptor-ligand bonds.

Cooperative Binding of Membrane Receptors

A direct consequence of the equations (3) and (4) is the quadratic dependence

$$[RL] \approx c(\kappa/k_B T) l_{we}^2 K_b^2 [R]^2 [L]^2 \quad (5)$$

of the bond concentration $[RL]$ on the area concentrations $[R]$ and $[L]$ of free receptors and ligands. This quadratic dependence indicates cooperative binding. The binding cooperativity results from a ‘smoothing’ of the thermally rough membranes and, thus, an increase of P_b with increasing concentrations $[R]$ and $[L]$ of receptors and ligands, which facilitates the formation of additional receptor-ligand complexes (see Fig. 2).

A consequence of eq. (5) is that the quantity K_{2D} defined in eq. (2) is not constant, but depends on the concentrations of the receptors and ligands. Eq. (5) thus helps to understand why different experimental methods to measure K_{2D} can lead to significantly different results [1].

T. Weikl, A. Bahrami, J. Hu, H. Kroboth, T. Rouhi
thomas.weikl@mpikg.mpg.de

References:

- [1] Kroboth, H., Rozycki, B., Lipowsky, R. and Weikl, T. R.: Binding cooperativity of membrane adhesion receptors. *Soft Matter* **5**, 3354-3361 (2009).
- [2] Weikl, T. R., Asfaw, M., Kroboth, H., Rozycki, B. and Lipowsky, R.: Adhesion of membranes via receptor-ligand complexes: Domain formation, binding cooperativity, and active processes. *Soft Matter* **5**, 3213-3224 (2009).
- [3] Rozycki, B., Lipowsky, R. and Weikl, T. R.: Adhesion of surfaces via particle adsorption: exact results for a lattice of fluid columns. *J. Stat. Mech.*, 211006 (2009).
- [4] Rozycki, B., Lipowsky, R. and Weikl, T. R.: Segregation of receptor-ligand complexes in cell adhesion zones: phase diagrams and the role of thermal membrane roughness. *New. J. Phys.* **12**, 095003 (2010).

MEMBRANES AND VESICLES

Aqueous Phase Separation in Vesicles: Wetting Phenomena and Nanotube Formation



Aqueous solutions containing two species of water-soluble polymers such as dextran and polyethylen glycol (PEG) undergo phase separation as soon as the polymer concentrations exceed a few weight percent, see **Fig. 1**.

Membranes and vesicles suspended in such a solution are then exposed to two different aqueous phases. Such lipid/polymer systems undergo complete-to-partial wetting transitions [1],

exhibit effective and intrinsic contact angles [2], and lead to the formation of membrane nanotubes [3].

Reinhard Lipowsky 11.11.1953

1978: Diploma, Physics,
(University of Heidelberg)

1982: PhD (Dr. rer. nat.), Physics
(University of Munich)

1979-1984: Teaching Associate
(University of Munich)

1984-1986: Research Associate
(Cornell University)

1986-1988: Group leader (FZ Jülich)

1987: Habilitation, Theoretical Physics
(University of Munich)

Thesis: Critical behavior of interfaces:
Wetting, surface melting and related
phenomena

1989-1990: Associate Professorship
(University of Munich)

1990-1993: Full Professorship
(University of Cologne), Director of the
Division "Theory II" (FZ Jülich)

Since Nov 1993: Director
(Max Planck Institute of Colloids and
Interfaces, Potsdam)

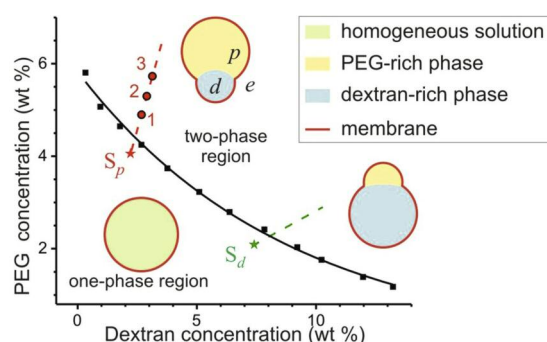


Figure 1: Phase diagram of aqueous solution of PEG and dextran. The solution undergoes phase separation into a PEG-rich phase p and a dextran-rich phase d as soon as the concentration of one of the polymers exceeds a few percent. The black line represents the binodal, i.e. the boundary between the one-phase and the two-phase region. The red and the green lines indicate two different deflation trajectories starting from two initial states S_p and S_d in the one phase region.

A convenient method to induce phase separation within the vesicles is by osmotic deflation. Osmotically active particles such as sugar molecules are added to the exterior solution, and the resulting osmotic unbalance leads to the permeation of water through the vesicle membranes and to a reduced volume of the vesicles. Since the dissolved polymers cannot permeate the membrane, the polymer concentration is increased, and the aqueous solution within the vesicle forms two separate phases, a PEG-rich and a dextran-rich phase, see **Figs. 2** and **3**.

In **Fig. 2**, the aqueous solution within the vesicle is initially homogeneous, see **Fig. 2(a)**, and then forms, during successive deflation steps, a dextran-rich droplet (light green) and a PEG-rich droplet (dark green), see **Fig. 2(b) - (f)**.

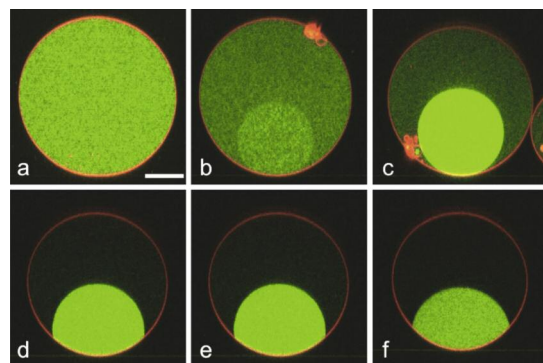


Figure 2: Confocal micrographs of a lipid vesicle (red line) which encloses a PEG-rich droplet (dark green) and a dextran-rich droplet (light green). As the vesicle is deflated from (c) to (d), the membrane undergoes a transition from complete to partial wetting by the PEG-rich phase. Further deflation from (d) to (f) leads to an increasing value of the contact angle between the membrane and the PEG-rich phase. Scale bar: 20 μm . [1]

Inspection of **Fig. 2** shows that the contact angle between the PEG-rich droplet and the membrane is close to zero for small deflation as in **Fig. 2(b)** and **(c)** but starts to increase for larger deflation as in **Fig. 2(d) - (f)**. Therefore, the system undergoes a complete-to-partial wetting transition as the vesicle is deflated from **Fig. 2(c)** to **(d)**.

The vesicle shapes shown in **Fig. 2(d) - (f)** are somewhat special since they stay essentially spherical even though the membrane is partially wet by both phases. In general, partial wetting of the membrane leads to a kink along the contact line, at which the membrane is pulled by the interface between the PEG-rich and dextran-rich phase, see **Fig. 3(a)**. In all cases, this contact line divides the membrane into two distinct segments, separating the two aqueous phases, α and β , within the vesicle interior from the exterior solution, γ . In general, these two membrane segments experience two

distinct mechanical tensions, $\Sigma_{\alpha\gamma}$ and $\Sigma_{\beta\gamma}$. In mechanical equilibrium, these two tensions must be balanced, along the contact line, by the interfacial tension $\Sigma_{\alpha\beta}$ between the two liquid phases, see **Fig. 3(a)** and **(b)**.

The kink shown in **Fig. 3(a)** is observed by optical microscopy but cannot persist to small length scales, since such a kink would imply an infinite bending energy of the membrane. Therefore, when viewed with suboptical resolution, the membrane must be smoothly curved as in **Fig. 3(b)**, which implies the existence of an intrinsic contact angle Θ_{in} . In contrast to the three contact angles shown in **Fig. 3(a)**, the intrinsic contact angle represents a material parameter that is independent of the vesicle geometry. **[2]**

Another unexpected aspect of the aqueous phase separation within the vesicles is the formation of membrane nanotubes, see **Fig. 4**. The tubes have a diameter below optical re-

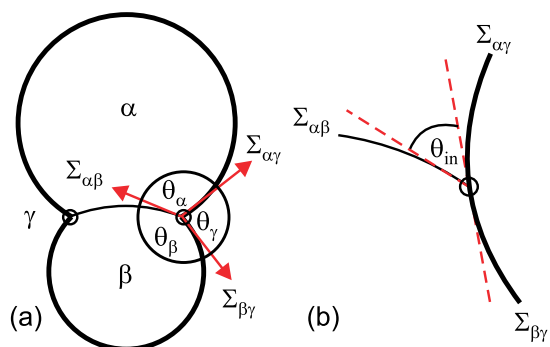


Figure 3: (a) Cross-section of a vesicle enclosing one α (top) and one β (bottom) droplet suspended in the exterior solution γ . When viewed with optical resolution, the vesicle shape exhibits a sharp kink along the contact line (\odot) and can be characterized by three effective contact angles θ_α , θ_β , and θ_γ . These contact angles are related to the three tensions $\Sigma_{\alpha\beta}$, $\Sigma_{\alpha\gamma}$, and $\Sigma_{\beta\gamma}$ via the force balance along the contact line; and (b) Enlarged view close to the contact line: Intrinsic contact angle Θ_{in} between the two planes that are tangential to the α_β interface and to the smoothly curved vesicle membrane, respectively, at a certain point of the contact line. **[2]**

solution and become only visible when fluorescently labeled. The tubes form during the phase separation process and are stable after this process has been completed **[3]**. A theoretical analysis of the deflated vesicles reveals that these membrane tubes are stabilized by negative spontaneous curvature. Using the large separation of length scales between the tube diameter and the overall size of the vesicles, the spontaneous curvature can be calculated and is found to be about $-1/(240 \text{ nm})$ for a certain range of polymer concentrations. The nanotubes can also be retracted back into the mother vesicle by increasing the membrane tension via micropipette aspiration of the vesicle.

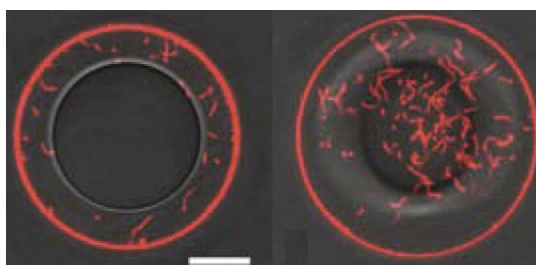


Figure 4: Membrane nanotubes (short red segments) extending from the vesicle membrane (red circle) into the vesicle interior. The nanotubes are below optical resolution and only visible when fluorescently labeled. These tubes are induced by the aqueous phase separation and stabilized by the spontaneous curvature of the membranes. The latter curvature is negative and about $-1/(240 \text{ nm})$. The tube may then have a cylindrical shape with radius 120 nm , a necklace-like morphology consisting of small spheres with a radius of 240 nm , or some intermediate morphology. **[3]**

R. Lipowsky, R. Dimova, H. Kusumaatmaja, Y. Li

References:

- [1]** Y.H. Li, R. Lipowsky, and R. Dimova. Transition from complete to partial wetting within membrane compartments. *JACS*, **130**:12252–12253, 2008.
- [2]** H. Kusumaatmaja, Y.-H. Li, R. Dimova, and R. Lipowsky. Intrinsic contact angle of aqueous phases at membranes and vesicles. *Phys. Rev. Lett.*, **103**: 238103, 2009.
- [3]** Y.-H. Li, R. Lipowsky, and R. Dimova. Membrane nanotubes induced by aqueous phase separation and stabilized by spontaneous curvature. *Proc. Nat. Acad. Sci. USA*, **108**: 4731-4736, 2011.

Stochastic Processes in Complex and Biological Systems



Molecular Motors as Semi-Markov Chains

Kinesin is a complex molecular machine whose properties have been studied in great detail both theoretically and experimentally in our department [1, 2]. When we experimentally observe a kinesin molecule walking along a filament, we see a series of forward and backward steps, whose relative frequency depends on the availability of ATP, the fuel of this motor. A more detailed analysis reveals, however, that the steps of the kinesin motor are more complex. In fact, both the probability of a motor to make a step forward or backward and the time that it takes to perform one of these steps depend on whether the motor had previously performed a forward or backward step. A detailed analysis of these different probabilities was done in [3], where we showed that the motor's displacements should be described in terms of pairs of steps, such as bf which means a step backward followed by a step forward. It turns out, therefore, that there are four such states indicated as $\{ff, fb, bf, bb\}$. In this representation, the motor is described as a stochastic chain in continuous time over these four states with the property that the dwell times are not exponentially distributed. These chains are called semi-Markov chains. Since the dwell times on these four states are also experimentally accessible and this level of description may apply to a large class of motors, we want to develop a mathematical framework to analytically compute several properties that are also easily accessible experimentally. This project is performed in collaboration with Prof Sylvie Rœlly at the University of Potsdam.

A. Valleriani, P. Keller, R. Lipowsky

Models for Translational Control

Translation of the messenger RNA (mRNA) is a key process in cell biology. The process of translation is performed by ribosomes, which are molecular machines walking unidirectional on the mRNA while synthesizing the proteins. The amount of proteins produced by each mRNA depends therefore on the number of ribosomes on it, which depends on the initiation rate, on the speed by which the ribosomes move along the chain, and on the termination rate. Finally, the number of ribosomes depends also on the life time of the mRNAs. Our work is mainly concerned with the bacterium *E. coli*. Experimentally, in collaboration with Prof Zoya Ignatova at the University of Potsdam, we are determining the number of ribosomes on certain mRNAs and we are preparing the samples for a ribosomal footprinting over the whole set of mRNAs in this organism. From the theoretical side, we have found out

that the kind of mRNA degradation pathways in *E. coli* cells has some effect both on the number of ribosomes and also on the rate of protein synthesis and that this effect is stronger for longer mRNAs [4, 5, 6]. In our theory, simple models of mRNA degradation have shown that some differences in the process of degradation can have dramatic effects on the translation rate (see Fig. 1). We are therefore developing more complex models based on the available knowledge about the degradation process in order to finally understand the role of degradation on the rate of protein synthesis [7]. On the other hand, under certain circumstances the tRNAs necessary to perform the translation can become particularly rare and thus slow down the ribosomes at certain positions along the mRNA [8]. We are thus developing a model to take properly into account the effective concentrations of all tRNAs and thus predict the local speed of the ribosomes and compare these results with the experimental footprinting.

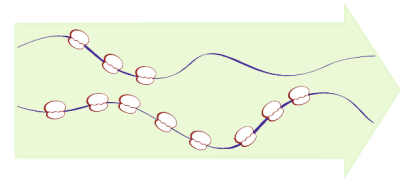


Fig. 1: Schematic diagram of mRNA translation at different times. The two chains have the same length but differ in the number of loaded ribosomes. The upper chain is young and has only few ribosomes that are close to the initiation region. The chain at the bottom is older and thus is loaded with more ribosomes. The arrow indicates the direction of motion of the ribosomes. If mRNA turn-over is very rapid, some mRNA may be degraded before producing any protein.

A. Valleriani, A. Nagar, I. Fedyunin, C. Deneke, S. Rudorf, R. Lipowsky

Life Cycle of Chlamy Cells

Chlamydomonas reinhardtii (chlamy) is a unicellular photosynthetic alga that is studied within the ongoing systems biology project GoFORSYS, in collaboration with the University of Potsdam and the MPI of Plant Physiology (MPIMP). Chlamy cells have the special property that they remain in the growth phase for a random amount of time and attain, at a population level, a relatively broad distribution of cell sizes. One consequence is that each mother cell can produce a number of daughter cells that is roughly proportional to the logarithm of its size (see Fig. 2). Since cell volume is often

considered as a proxy for the cellular metabolic state, the first objective is therefore to develop a model for the cell size distribution under time-independent conditions such as those found in the bioreactor at the MPIMP. The model can be used to calculate and compare stationary distributions for the common binary and the multiple division processes [9].

We have also addressed another set of experiments that were performed in the labs of Prof Martin Steup at the University of Potsdam. In these experiments, the cells are synchronized by fixed periods of light and darkness and are grown in a special medium that does not allow for cell growth in the darkness. Synchronization relies on the fact that, under certain general conditions, all cells would divide after the start of the dark period and the daughter cells would start to grow only when light is turned on again. These experiments allow determining the relationship between the cell size and the number of daughter cells as well as the cell growth rate and the timing of DNA replication. Our current aim is to use our model to predict the cell size distribution at the beginning of the light period.

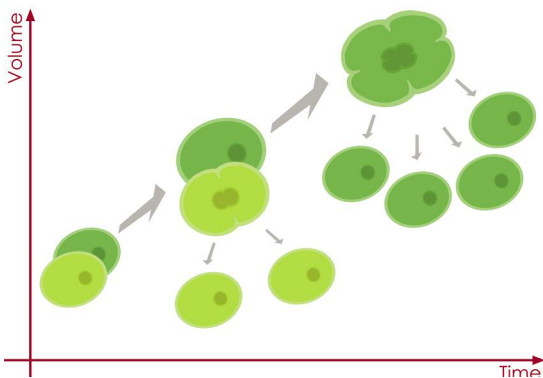


Fig. 2: Multiple cell division. Two twin cells grow in volume over time but one cell divides earlier than the other. The first dividing cell (light green) is relatively small at division time and produces only two daughter cells. The cell that divides later (dark green) attains a larger volume and can divide in four daughter cells. In the cell culture, one can observe also large mother cells producing up to 32 daughter cells.

A. Valleriani, M. Rading, R. Lipowsky

Patterns on Complex Networks

In this research activity, we consider networks as collections of points, called vertices, connected by bi-directional links, sometimes also called edges. Random networks are those networks in which the number of edges connected to any

randomly chosen vertex, which is called the degree of the vertex, is a random variable that follows a given distribution. This distribution is called the degree distribution of the network. A special subset of these random networks is given by those characterized by a power law degree distribution. Random networks are sometimes called complex networks and all known complex networks have a direct or indirect biological origin. Prominent examples are food webs, as well as social and neural networks.

In general, the vertices of biological networks are dynamic and exhibit various properties or internal degrees of freedom that evolve with time. A proper description of the network is then obtained in terms of dynamical variables that are defined for each vertex of the network. In a neural network, for instance, the vertices represent firing and nonfiring neurons and thus switch between an active and an inactive state depending on the signals that arrive from the neurons connected to them.

In general, the dynamics of each vertex is determined by the local interactions of this vertex with its neighbors. One instructive example is provided by local majority rule dynamics which is defined as follows: If, at a certain time, most direct neighbors of a certain vertex are active or inactive, this vertex will become active or inactive at the next update of the pattern. One interesting question concerns the result of the update rule once it is repeated many times over the whole networks. In particular, we would like to estimate the number of attractors of the dynamics. We have found out that the knowledge of the degree distribution alone is not sufficient to provide a general answer. Indeed, it turns out that the degree-degree correlation between the vertices plays a major role.

It is perhaps for this reason that most naturally occurring networks have either positive or negative degree-degree correlation. In both cases, the activity patterns are governed by a large number of attractors. In fact, we have found out that in dissortative scale-free networks the number of attractors exhibits a maximum as a function of network size [10], while in assortative networks the number of attractors steadily increases with network size [11]. We have indeed found out that the structure of the network takes a peculiar nested form that depends on whether the degree correlation is positive or negative. This structure can be visualized in terms of partially connected subnetworks or layers of different size whose dynamics can be compared with that of Ising models in different dimensions [12].

A. Valleriani, J. Menche, R. Lipowsky

References:

- [1] Lipowsky R. et al.: Active bio-systems: From single motor molecules to cooperative cargo transport. *Biophys. Rev. Lett.* **4**, 77 (2009).
- [2] Lipowsky R., Liepelt S., and Valleriani A.: Energy conversion by molecular motors coupled to nucleotide hydrolysis. *J. Stat. Phys.* **135**, 951 (2009).
- [3] Valleriani A., Liepelt S. and Lipowsky R.: Dwell time distributions for kinesin's mechanical steps. *EPL* **82**, 28011 (2008).
- [4] Valleriani A., Ignatova Z., Nagar A., and Lipowsky R.: Turnover of messenger RNA: Polysome statistics beyond the steady state. *EPL* **89**, 58003 (2010).
- [5] Valleriani A. et al: Length dependent translation of messenger RNA by ribosomes. Submitted for publication.
- [6] Nagar A., Valleriani A. and Lipowsky R.: Effect of mutual exclusion of ribosomes during protein synthesis with mRNA degradation. In preparation.
- [7] Deneke C., Valleriani A. and Lipowsky R.: The shielding effect of ribosomes against degradation of messenger RNA. In preparation.
- [8] Zhang G. et al: Global and local depletion of ternary complex limits translational elongation. *Nucl. Acid Res.* **38**, 4778 (2010).
- [9] Rading M., Lipowsky R. and Valleriani A.: The stationary size distribution of cells. In preparation.
- [10] Menche, J., Valleriani, A. and Lipowsky R.: Asymptotic properties of degree-correlated scale-free networks. *Phys. Rev. E* **81**, 046103 (2010).
- [11] Menche J., Valleriani A., and Lipowsky R.: Dynamical processes on dissortative scale-free networks. *EPL* **89**, 18002 (2010).
- [12] Menche J., Valleriani A., and Lipowsky R.: Sequence of phase transitions in Ising models on correlated networks. Submitted for publication.

Regulation of Bio-Processes



Most biological processes are tightly regulated. For example, the genetic information is processed in several steps, transcription, translation, and degradation of mRNA and protein. Each of these steps may be the target of regulatory mechanisms that switch a gene on or off or fine-tune the concentration of its product. Our group is interested in the design principles behind these control mechanisms and the underlying physical constraints, with a focus on bacterial systems. In general, we attempt to use theory as a way to bridge between molecular information and its macroscopic (physiological or evolutionary) context.

Stefan Klumpp 29.09.1973
1999: Diploma, Physics (University of Heidelberg)
 Thesis: Noise-induced transport of two coupled particles.
2003: PhD, Physics (University of Potsdam/MPI of Colloids and Interfaces, Potsdam)
 Thesis: Movements of molecular motors: Diffusion and directed walks
2004-2005: Research associate (MPI of Colloids and Interfaces, Potsdam)
2006-2009: Postdoc (University of California, San Diego)
since 2009: Group leader (MPI of Colloids and Interfaces, Potsdam)

Dynamics and Regulation of Transcription

The first step in gene expression is transcription by RNA polymerases (RNAPs) that move along a gene and synthesize an RNA copy of its sequence. The dynamics of this process is a complex interplay of stochastic stepping along the DNA and several types of pauses. One question we are interested in is how this complex dynamics affects transcription under conditions where a gene is transcribed by multiple RNAPs simultaneously. Dense RNAP traffic is typical for the transcription of ribosomal RNA (rRNA) in fast growing bacterial cells, as large ribosome concentrations are needed for the high rate of protein synthesis associated with rapid cell growth. Using lattice models that are related to simple exclusion processes from non-equilibrium statistical physics, we found that backtracking pauses (during which RNAPs slide backwards in a diffusive fashion) are strongly suppressed under these conditions, but that pauses without backtracking may severely limit the transcription rate (**Fig. 1**) [1]. Rapidly growing cells therefore need to actively suppress such pauses. In bacteria, this is achieved by the so-called ribosomal antitermination system.

The suppression of backtracking pauses in dense RNAP traffic may also be used in regulatory mechanisms: If pausing is coupled to the termination of transcription, the probability of termination can be modulated by the pause duration and, thus, by the transcription rate [2]. As a result, transcription can become very sensitive to changes in the rate of transcription initiation.

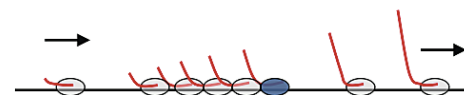
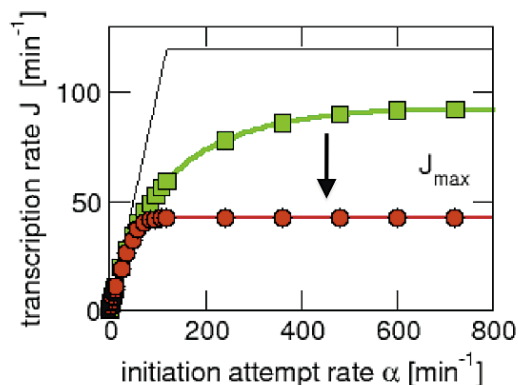


Fig. 1: Pauses during transcription reduce the maximal transcription rate (green to red) due to traffic jams behind paused RNAPs.

Economic Principles of the Transcription and Translation Machinery

RNAPs as well as ribosomes, the molecular machines of translation, are allocated by the cell to genes or classes of genes based on the requirements of their genetic program. For RNAPs, we have used a functional partitioning model (**Fig. 2**) to study this allocation. The model indicates that there is a large pool of RNAPs that are non-specifically bound to DNA. This pool buffers the concentration of free RNAPs against changes in transcription of even highly transcribed genes such as the rRNA genes. Therefore, even dramatic changes in the transcription of a class of gene only weakly affect other genes [3].

Ribosomes underlie different economic principles, as most ribosomes in bacterial cells are active in translation and their activity is directly linked to cell growth. Optimizing ribosome activity therefore provides a fitness advantage, which we have used as a basis to understand the non-random usage of synonymous codons (different nucleotide triplets encoding the same amino acid). An evolution model for codon usage allows us to obtain a prediction of the abundance of a protein from codon frequencies in the sequence of its gene.

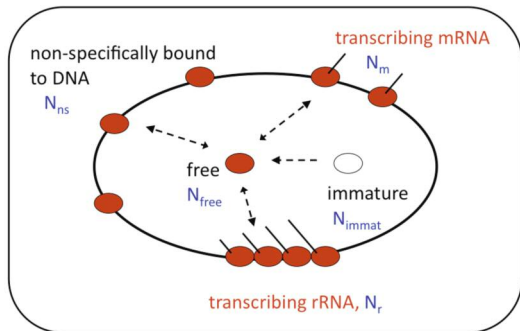


Fig. 2: Model for the partitioning of RNA polymerases into five functional classes.

Genetic Circuits and Growth-Rate Dependent Gene Expression

The control networks of genes regulating other genes are often described in analogy to electrical circuitry. However, genetic circuits remain coupled to the physiological state of their host cell, which for example provides the machinery of gene expression. As a result, the concentration of the product of a gene depends not only on its regulation but also on the state of the whole cell, which in bacteria can often be characterized by the growth rate. We have characterized the growth rate dependence of gene expression of unregulated genes (Fig. 3) and several simple circuits [4]. If the product of a gene also affects cells growth, these effects can give rise to a new feedback mechanism, mediated by a modulation of cell growth. Such feedback, due to the controlled expression of chromosomal toxins may have a role in the establishment of tolerance against antibiotics (persistence) [4].

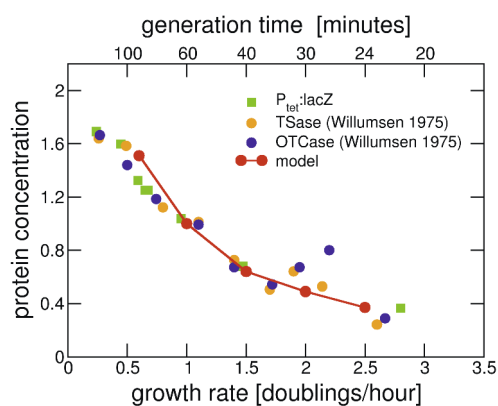


Fig. 3: Growth-rate dependence of gene expression for an unregulated gene, theoretical results (red line) and experimental data for several systems (symbols).

Cooperative Molecular Motors

We have also continued our activity in modeling the cooperative action of small teams of molecular motors. Using detailed simulations of a bead pulled by several kinesin motors [5], we studied how cooperative transport depends on mechanical aspects of the system (collaboration with the group of Ulrich Schwarz, University of Heidelberg). Surprisingly, there is a rather robust relation between the average number of pulling motors and the processivity (run length) of the bead, in good agreement with our earlier model (Fig. 4). The increase in processivity with increasing number of motors is also found for motors pulling in opposite directions, despite the tug-of-war between two teams of motors [6].

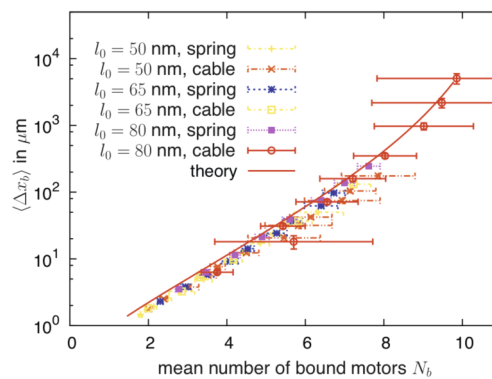


Fig. 4: Run length of a bead transported by several kinesin motors as predicted by simulations that vary the geometrical and mechanical properties of the motors.

S. Klumpp, M. Faber, R. Marathe, M. Mauri, M. Sahoo, P. Patra, klumpp@mpikg.mpg.de.

References:

- [1] Klumpp, S., Hwa, T.: Stochasticity and traffic jams in the transcription of ribosomal RNA: Intriguing role of termination and antitermination. Proc. Natl. Acad. Sci. USA **105**, 18159-18164 (2008).
- [2] Klumpp, S.: Pausing and backtracking in transcription under dense traffic conditions. J. Stat. Phys. Published online (2011), DOI: 10.1007/s10955-011-0120-3
- [3] Klumpp, S., Hwa, T.: Growth-rate dependent partitioning of RNA polymerases in bacteria. Proc. Natl. Acad. Sci. USA **105**, 20245-20250 (2008).
- [4] Klumpp, S., Zhang, Z., Hwa, T.: Growth-rate dependent global effects on gene expression in bacteria. Cell **139**, 1366-1375 (2009).
- [5] Korn, C.B., Klumpp, S., Lipowsky, R., Schwarz, U.S.: Stochastic simulations of cargo transport by processive molecular motors. J. Chem. Phys. **131**, 245107 (2009).
- [6] Müller, M.J.L., Klumpp, S., Lipowsky, R.: Bidirectional transport by molecular motors: Enhanced processivity and response to external forces. Biophys. J. **98**, 2610-2618 (2010).